ELSEVIER

Contents lists available at ScienceDirect

Journal of the European Ceramic Society

journal homepage: www.elsevier.com/locate/jeurceramsoc





Interphase boundary, grain boundary, and surface diffusion in Al₂O₃-GdAlO₃ composites determined from bicrystal coble creep experiments

D. Keith Coffman ^a, Yonghui Ma ^{b,c}, Christopher M. Barr ^d, Jia-hu Ouyang ^b, Khalid Hattar ^d, Shen J. Dillon ^{a,e,*}

- ^a Department of Materials Science and Engineering, University of Illinois at Urbana-Champaign, Urbana, IL 61801, USA
- ^b School of Materials Science and Engineering, Harbin Institute of Technology, Harbin 150001, China
- ^c Yantai Research Institute and Graduate School of Harbin Engineering University, Yantai, Shandong 264006, China
- ^d Materials, Physical, and Chemical Sciences, Sandia National Laboratories, Albuquerque, NM 87185, USA
- ^e Department of Materials Science and Engineering, University of California, Irvine, CA 92697, USA

ARTICLE INFO

Keywords: in situ Transmission electron microscope Alumina Gadolinium aluminate Diffusivity

ABSTRACT

Small-scale in situ transmission electron microscopy-based Coble creep experiments were performed on Al₂O₃-GdAlO₃ composites using localized laser heating. A primary goal of the work was to isolate the Al₂O₃-GdAlO₃ interphase boundary diffusivity in order to understand how it contributes to the average properties of the composite. The diffusivities of the grain boundaries (GB) of GdAlO₃ (GAP) and Al₂O₃ were measured to be $D_{Gb,GAP} = (15 \pm 14) \exp \left(\frac{-580,000 \pm 62,000 \text{Jmol}^{-1}}{RT} \right) m^2 \quad s^{-1}$, and $D_{GB,Al_2O_3} = (25 \pm 21) \exp \left(\frac{-542,000 \pm 30,000 \text{Jmol}^{-1}}{RT} \right) m^2 \quad s^{-1}$, respectively. The average interphase boundary (IPB) diffusivity exceeds that of the grain boundaries and was measured to be $D_{IPB} = (15 \pm 14) \exp \left(\frac{-559,000 \pm 117,000 \text{Jmol}^{-1}}{RT} \right) m^2 \quad s^{-1}$. Capillary smoothing experiments after creep were used to determine surface (S) diffusivities, $D_{S,Al_2O_3} = \left(3.2 \times 10^3 \pm 2.7 \times 10^3\right) \exp \left(\frac{-539,000 \pm 26,000 \text{Jmol}^{-1}}{RT} \right) m^2 \quad s^{-1}$ and $D_{S,GAP} = \left(4.6 \times 10^4 \pm 7.7 \times 10^{-6}\right) \exp \left(\frac{-625,000 \pm 82,000 \text{Jmol}^{-1}}{RT} \right) m^2 \quad s^{-1}$. This works demonstrates the feasibility of small-scale Coble creep experiments to directly measure individual components of grain boundary and IPB diffusivities in composites.

1. Background

Diffusion along crystalline interphase boundaries affects the processing and properties of materials in a variety of applications such as sintering composite materials, stress relaxation at metal-oxide interfaces during high temperature oxidation, the morphological evolution of precipitates, dewetting of thin films, or creep of composites [1–4]. Despite the general importance of diffusion at interphase boundaries, relatively few measurements of interphase boundary diffusion have been reported in the literature [5]. The dearth of data consequently underlies a generally poor understanding of their diffusion [6].

This work focuses on measuring all the average rate-limiting interfacial diffusivities in the $\alpha\text{-alumina}$ (corundum, $\text{Al}_2\text{O}_3\text{)-gadolinium}$ aluminate perovskite (GAP, GdAlO_3) system. Alumina-rare-earth aluminate composites and eutectic composites have received considerable interest as potential creep resistant high temperature materials for structural applications [7–13]. Polycrystalline composites, such as alumina-yttrium aluminum garnet (YAG), tend to creep at lower rates than the pure single-phase component systems [8,9,12,13]. The composites, however, do not necessarily exhibit slower creep than the doped single-phase systems [14,15]. The composites naturally contain doped grain boundaries whose kinetics may be suppressed by segregation of

^{*} Corresponding author at: Department of Materials Science and Engineering, University of California, Irvine, CA 92697, USA. *E-mail address:* sdillon1@uci.edu (S.J. Dillon).

the secondary component [16]. As a result, it is difficult, for example, to determine whether the ${\rm Al_2O_3}$ -YAG interfaces suppress diffusional transport, topological effects dominate the creep response, dopant chemistry plays the most important role, or some combination of these factors. Since the doped, undoped, and composite systems coarsen differently during experiments and can display different stress dependencies in different grain size regimes and temperatures, single variables are challenging to isolate in conventional experiments. The data can, therefore, be challenging to interpret in the context of fundamental materials properties such as interfacial and grain boundary diffusivity. This example highlights various challenges that often arise in the context of interpreting diffusion dependent transport mechanisms in crystalline composite systems at high temperatures.

Diffusion along phase boundaries is challenging to measure via methods traditionally applied to the simpler case of grain boundary diffusion, since long-range tracer diffusion in a composite structure is difficult to fit to a simple model [17]. As a result far fewer measurements of interphase boundary diffusion have been made, although a number of such data are summarized in reference [5]. No simple trends emerge from the data [5]. For example, tracer diffusion measurements along interfaces in eutectic colonies in Pb-Sn alloys suggest that the interphase diffusivity of the two components are approximately equivalent, but 2-3 orders of magnitude slower than gain boundary diffusion in the system [18]. Alternatively, diffusivity along $\alpha - \beta$ interfaces in Zr indicate that interphase boundary diffusivity and grain boundary diffusivity are of comparable magnitude [19]. Oxygen and potassium diffusivity at feldspar-quartz interfaces was measured to exceed the grain boundary values in the component materials [20]. Detailed bicrystal tracer experiments have been performed along Sn-Ge interfaces, which demonstrate considerable anisotropy with respect to interface type [21]. Measurements at Cu-Ag interfaces indicate that directional anisotropy in diffusivity also exists at individual interfaces [22].

Alternative microstructural evolution-based experimental methods have also been developed to characterize interphase boundary diffusion. For example, diffusion at Al₂O₃-metal interfaces has been discussed in multiple investigations of dewetting behavior of metallization [3]. Indirect measurements and computation suggest that diffusivity along metal-oxide interfaces may be comparable to that along high angle grain boundaries in metals [6]. Au chemical tracer measurements have been performed at Al₂O₃-Ni interfaces along thin film interfaces using energy dispersive spectroscopy based chemical mapping. The phase boundary was found be \approx 4 orders of magnitude slower than Au diffusion at Ni grain boundaries, \approx 4 orders of magnitude faster than Au lattice diffusion in Ni, and far in excess of the grain boundary diffusivity of Al₂O₃, which is effectively zero ≈ 500 °C where the experiments were performed [23]. The results imply, as might be anticipated that Au primarily diffuses along the metal interface. At metal-metal interfaces or oxide-oxide interfaces it would be valuable to understand how each portion of the phase boundary is contributing to the average behavior of the interface. Such data is, however, difficult to obtain through tracer measurements.

In recent work, our group demonstrated single grain boundary Coble creep-based measurements of grain boundary diffusivity in $\rm ZrO_2$ using small-scale high temperature mechanical testing [24,25]. Nanowire growth occurs during single grain boundary tensile Coble creep, where atoms at the surface diffuse into the grain boundary that is under tensile stress. Similar experiments have also been reported for Al [26] and Ni [27], although the responses were primarily attributed to thermal gradient and electric fields, respectively. Analogous Coble creep experiments performed on interphase boundaries should similarly result in nanowire growth but form heterophase nanowires where the relative amounts of each phase grown will scale with their relative contribution to the interphase boundary diffusivity. It has been previously shown that interphase diffusion at diamond-metal nanoparticle contacts is important in the so-called pseudo-elastic response of very fine metal nanoparticles during compression, which accounts for a Coble creep-like

response of the surfaces and interfaces of small nanoparticles deformed at room temperature [28]. Performing related experiments on bulk samples at higher homologous temperatures along with in situ imaging, that allows the data to be easily quantified, will enable related methodologies to directly measure the relative contributions of each phase to interphase boundary diffusion. Analogous measurements of grain boundary diffusivity from the component phases and surface diffusivity may also be obtained from the same series of experiments, which can provide greater context for interface diffusion in the composite system.

This work represents an initial attempt to isolate the various interfacial diffusivities in a composite system in order to better understand how the average interphase boundary diffusion compares to grain boundary and surface diffusion in the component systems of the same chemistry. The general results provide context for understanding the average transport kinetics in Al_2O_3 -rare earth aluminate composites.

2. Experimental procedure

Nanoscale Al₂O₃-GAP powder was synthesized at the eutectic composition via chemical co-precipitation described in detail elsewhere [29]. This powder was well mixed with 10 vol% 500 nm α -SiC (St-Nano Science & Technology Co., Ltd, Shanghai, China; 99.9%) by wet-ball milling for 24 h. Afterwards, the mixed powder was hot-pressed to form a dense pellet at 1500 °C for 1 h with 30 MPa uniaxial pressure (Advanced Vacuum System, AVS-2200, AVS Inc., USA). The sample preparation resulted in nanograins of both α-Al₂O₃ and GdAlO₃ and contained dispersed SiC particles. SiC was initially included to aid IR absorption, but was present at low enough phase fraction to be avoidable during interfacial diffusion measurements. Later experiments, however, demonstrated that the presence of SiC was not necessary to obtain effective optical heating. The microstructure of these same samples was characterized in prior work [30]. The grain sizes of the Al_2O_3 and $GdAlO_3$ phase were $\approx 1~\mu m$. The $\approx 500~nm$ diameter SiC should appear as a light phase like Al₂O₃ in the TEM images due to their similar density. Thin sections were prepared by cutting with a diamond saw and polishing using diamond lapping films. The result was a wedge-shaped sample approximately 3 mm long and 3 mm wide with an edge thickness of $< 50 \mu m$. A portion of the sample was further cut at an angle to produce a needle-shaped sample approximately 3 mm long. The needle-shaped sample was mounted on a piece of Ti and placed on the indenter portion of a Bruker/Hysitron PI-95 picoindenter and the wedge-shaped sample was mounted on Cu mount and placed on the sample side of the mechanical tester. The samples were coated with a thin layer, \approx 3–5 nm, of Au-Pd. Trace amounts of Au-Pd could be present in the vicinity of the experimental measurements, but these atoms would be in the metallic state under the conditions tested and have effectively no solubility in the oxide. This material evaporates in the region irradiated by the laser, see supplementary Figure S1, but still provides for an enhanced conductive pathway to ground. Prior work on ZrO₂ utilized FIB prepared tips and pillars, however, it was found that asperity contacts could be made without the need for site specific preparation. Therefore, no further sample preparation was required.

Experiments were performed in a highly modified JEOL 2100 LaB₆, i. e. the I³TEM at Sandia National Laboratories, operated at 200 kV. The laser was set in approximately colinear alignment with the electron beam. Experiments were performed using a load-displacement data acquisition rate of ≈ 200 Hz and an in situ image acquisition rate of ≈ 7 Hz (Tietz video and image processing system). Electron irradiations performed on Al₂O₃ suggest that the threshold electron energy for displacement damage only occurs at ≈ 390 keV [31]. Thus, it is concluded that electron irradiation in our experiments, at 200 keV, should not induce displacement significant damage. That work observed a decrease in damage threshold around 600 °C, using fluxes of $\approx 10^4$ A/m² for 6 h, which resulted in nanoscale regions of metallic precipitates [31]. The displacement threshold should not, however, have a strong temperature dependence. The effect likely arises due to charging

of insulating samples, which can induce fields that drive diffusion and/or reactions at elevated temperatures. The Au-Pd film was deposited to support charge transport away from the region of observation, although it is noted that it evaporated from the area immediately below the laser spot. The adjacent film, nevertheless, provides an overall less resistive path for charge transport to ground. The experiments were all performed at relatively low magnification, less than 10,000x, where the electron beam current density is relatively low, $<10~{\rm A/m}^2,$ the timescale of most experiments is relatively short, e.g. $<5~{\rm min}$. The total dose is, thus 5–6 orders of magnitude lower than necessary to induce measurable damage.

The samples were heated using a 1064 nm wavelength IR laser focused to a spot size $\approx 50 \ \mu m$ in diameter operated at applied powers between 4 W and 5.3 W. The laser repetition rate, 33 kHz, is fast relative to the thermal relaxation time of the sample, due to the sample's high thermal impedance. The sample is, therefore, anticipated to achieve a continuous temperature at steady state. In prior work, the laser powertemperature calibration was found to be linear above the onset of emission at ≈ 1.6 W, based on electrical resistance measurements [32]. At 5.3 W, the Al₂O₃-GAP samples melt and evaporate under the laser irradiation. The sample primarily evaporates rapidly, but the regions adjacent to the evaporated material were found to contain eutectic Al₂O₃-GAP indicating that this material had melted and recrystallized (see supplementary Figure S1). All experiments were performed in the region shown in Figure S1 prior to melting. At 5.3 W, the sample temperature is referenced to the eutectic melting temperature, T_e = 1720 °C. A linear temperature response between 1.6 W and 5.3 W is assumed here as the basis for the temperature calibration. The linear response is apparent in lattice parameter expansion measurements obtained from electron diffraction; see supplementary Figure S2. Observations of surface diffusion from the two sides of the sample, suggested that the temperature on each side may be slightly different when out of contact. The laser can be used to evaporate the sample in situ, as shown in Figure S1, and observe its position, which enables good alignment with the electron beam. Differences in thermal impedance of each side of the specimen can, nevertheless, lead to temperature gradients. In order to understand the potential nature of any temperature differences or gradients a series of finite element analyses were performed using COMSOL. The analysis is summarized in the supplementary information, Figure S3. Even if the temperature difference between the two pieces of sample is relatively large when out of contact this is reduced to a relatively small gradient when in contact. The simulations, for example, suggest that at the resolution of our alignment a temperature difference on the order of 50 $^{\circ}$ C to 100 $^{\circ}$ C could exist when the pieces are out of contact but reduces to a small gradient, e.g. $\approx 1-2$ °C/ μ m, when in contact. This appears to be qualitatively consistent with our observations, wherein the surface diffusivity of the indenter portion of the sample was consistently lower by ≈ 100 –150 °C.

In prior work on ZrO_2 [24,25], it was found that point contacts between two pieces of material could induce sintering in situ, which could be followed by creep experiments. In the current work, it is possible to test Al_2O_3 - Al_2O_3 , GAP-GAP, and Al_2O_3 -GAP contacts of random misorientation. Samples were initially brought into contact for several seconds before being tested in tension under displacement control at rates between 5 nm s⁻¹ and 30 nm s⁻¹. The loading schedule of the indenter requires that it return to its initial position, which often leaves the resulting features in highly non-equilibrium geometries. The capillary relaxations can be measured to determine surface diffusivity, but also produce sharp asperities that can be used to establish contacts in subsequent experiments.

The precision of the Bruker/Hysitron PI-95 is $\approx 0.4~\mu N$ and its accuracy is $\approx 1~\mu N$. The loads during steady-state creep of the nanostructure are small relative to the accuracy of the measurement, since the interfacial radii are fixed by diffusion limitations and are typically on the order of 100 nm. Consequently, the general sintering stress, $\sigma_s = 2\gamma_s/r$, is used to approximate the applied stress during creep, where r is

the neck radius of curvature and γ_s is the surface energy. However, this is taken as a tensile stress rather than a compressive stress, which is in effect a stress of $-2\sigma_s$. This is reasonably in line with prior work on $\rm ZrO_2$, which measured creep under constant load conditions in order to determine the zero-creep stress [33]. This is the condition where the tensile load equals the sintering stress. A cylindrical grain solution to this condition is discussed here for simplicity [34], to demonstrate the reasoning behind use of the sintering stress as a basis for approximating the applied stress. The geometric approximation leads to; $\gamma_s = \frac{F}{\pi R k}$, where

 $\kappa = \left(1 - \frac{\gamma_{gb}}{\gamma_s}/\frac{2L}{R}\right)$. The condition is determined from the applied force, F, the cylinder radius, R, the dihedral angles, i.e. $\frac{\gamma_{gb}}{\gamma_{c}}$, and the length of the grains, L. Our prior experiments on ZrO2 probed contacts of comparable length scale to the current work, and it was found that all grain boundary contacts became unstable, i.e. rapidly thinned down and debonded, or failed via fracture for $\frac{F}{\pi R_{Y}} > 4.5 \gamma_{s}$ [24]. It is, thus, anticipated that steady-state behavior may not be observed for values significantly exceeding a value of this magnitude. This value is similar to the Johnson-Kendall-Roberts adhesion stress for asperity contacts in the reversible elastic regime of $\sigma_{ad} = 3\gamma_s/r$ [35]. Our calculated load is taken to be $F = 2\gamma_s \pi R \kappa$, since half of this value is the sintering stress. This value is within a factor of 3 of an anticipated maximum stress. This, however, represents an upper bound on the stress, which could give rise to potential concerns about overestimating the stress. Prior work on ZrO2 demonstrated that the system exhibits interface rate limited kinetics below a critical stress and only exhibits steady-state creep above a critical stress [24,25]. This phenomenon was observed in both creep and sintering experiments, and both sets of experiments produce consistent activation volumes. Similar phenomena were observed for large area contacts in tension here, but it was not possible to distinguish which phases were in contact outside of the steady-state creep experiments, and were, thus, not analyzed in detail. However, the interface rate limited sintering kinetics were investigated in detail and are the subject of a future manuscript. The effective critical stress, which is rate dependent with an exponential probability distribution, separating the interface rate limited and diffusion limited kinetic regimes is temperature dependent but $> 10^7$ Pa in the regime of interest in this work. To observe steady-state creep, the tensile stress should exceed this value. The range of possible stresses is somewhat finite, $10^7 Pa < \sigma = \frac{2\gamma_s \kappa}{R} < \frac{4\gamma_s \kappa}{R}$. This implies that steady-state creep would only be observed for contact radii on the order of ≈ 4 nm to ≈ 200 nm. In ZrO₂ steady-state creep was observed at a maximum contact radius of ≈ 300 nm at 2098 $^{\circ}\text{C}$ and a displacement rate of 20 nm s⁻¹, and steady-state creep was not obtainable at slower rates at this temperature. A minimum contact radius of \approx 5 nm was observed at 1604 °C and a displacement rate of 40 nm s⁻¹, and the boundaries pinched off during tensile loading at higher displacement rates. These data appear to be reasonably consistent with the approximation of creep stress. The calculated stresses in this work all fall within the range of 2×10^7 Pa to 5×10^8 Pa, which is in line with our predictions above. Averaging over all the experiments the stresses used for the Al₂O₃-GdAlO₃ interphase boundary, Al₂O₃ grain boundary, and GdAlO $_3$ grain boundary calculations were 5.1 \times 10 7 \pm 3.5 \times 10 7 Pa, 1.6 \times $10^8 \pm 0.7 \times 10^8 Pa$, and $3.6 \times 10^8 \pm 1.3 \times 10^8 Pa$, respectively. Although this calculation of stress is an approximation, it has reasonably narrow bounds. Errors for any interface type should be systematic, and systematic errors between interface types would not be large enough to change any of the general trends discussed in this work.

 γ_s is also not known explicitly. It has been measured to be between $\approx 0.4~\mathrm{J~m^{-2}}$ and $2~\mathrm{J~m^{-2}}$ for $\mathrm{Al_2O_3}$ depending on the amount of adsorbed $\mathrm{H_2O}$ [36]. Although the high temperature experiments performed in vacuum in this work are anticipated to be relatively anhydrous, the presence of adsorbed $\mathrm{Gd^{3+}}$ could also lower the energy. For simplicity, the assumed energy will be 1 J m⁻². The actual value for $\mathrm{Al_2O_3}$ surfaces is, therefore, anticipated to be within a factor of 2 of this value. The relative average energies of the other interfaces, γ_i , in the system will be

approximated by applying Herring condition under isotropic assumptions to the average measured dihedral angles, ϕ , i.e. $\frac{\gamma_1}{\gamma_c} = 2\cos\frac{\phi}{2}$.

A modified version of the Coble equation is used to calculate interfacial diffusivity, D_i . In the model, the atomic flux, J, is written as;

$$J = A \frac{\delta}{x^2} \frac{\Omega \sigma}{kT} D_i. \tag{1}$$

Here, k is the Boltzmann constant, T is temperature, σ is the stress, Ω is the molecular volume of a stoichiometric unit, x is the radius of the boundary, and A is the diffusional area, and δ is the interphase boundary width. The analysis used herein assumes a time constant, t_c , associated with inserting an atomic plane into a boundary of circular cross-section and radius, r. Where t_c is approximated by the displacement rate divided by the Burger's vector. This yields an equation for 2-D diffusion in the

interface at steady-state;

$$D_i = x^2 kT / 2\pi t_c \sigma \Omega, \tag{2}$$

which can be applied to calculating the contribution from each phase to the overall diffusivity of the interphase boundary.

The capillary relaxations of asperities evolved during the creep experiments are used as the basis for the measurements of surface diffusivity following the analysis of Nichols and Mullins [37]. The evolution of the radius of curvature, r, of conical tips is described by;

$$r_t^4 - r_{t,o}^4 = A_a \frac{D_s \gamma_s \Omega^2 \nu}{kT} (t - t_o) \tag{3}$$

where A_{α} is a geometric factor that both depends on the cone half-angle,

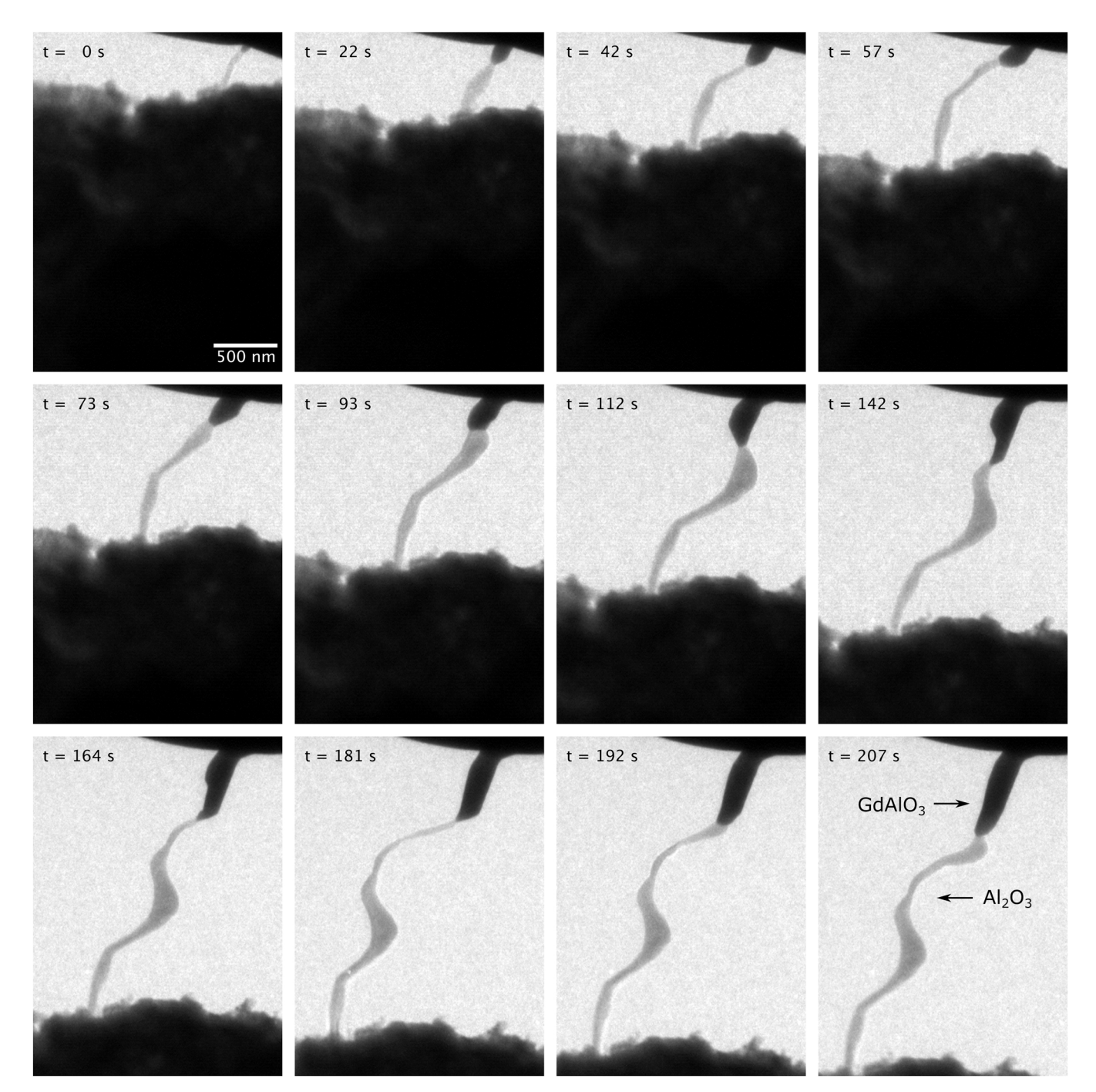


Fig. 1. Time-lapse images of in situ bicrystal Coble creep of Al_2O_3 -GdAl O_3 interface at a displacement rate of 10 nm s $^{-1}$ at $T\approx 1628~^{\circ}C$.

 ν is the concentration of surface diffusion mediating defects, D_s is the surface diffusivity, t is time, and γ_s is the surface energy, again assumed to be $\gamma_s \approx 1$ J m⁻².

Multiple experiments as well as multiple measurements from the same creep experiment taken at different points in time are averaged together to help reduce the error associated with this geometric assumption. The diffusivity values reported are obtained by averaging multiple measurements and the error bars are the standard deviation of the individual creep experiments at a single temperature. Image analyses were performed using the FIJI package of ImageJ and Matlab scripts.

3. Results

Fig. 1 and Videos S1-S2 show an example of a tensile Coble creep measurement performed on an Al₂O₃-GAP interphase boundary at 1628 °C and an imposed displacement rate of 10 nm s⁻¹. The measured load values are shown in Figure S4. Video S1 shows fitting of the center profile used to measure the length of the nanowire, while Video S2 shows fitting of the bounds of the nanowire along with the dihedral angle measurements. The brighter phase in the images is Al₂O₃ and the darker phase is GdAlO₃, the stack contrast difference results from their differing densities. The process results in the formation of a 2-phase nanowire heterostructure that grows via insertion of planes of atoms into the interface. The more facile surface diffusion allows the longerrange transport required for continuous growth. Fig. 2a plots the change in length of both the Al₂O₃ phase and GAP phase corresponding to the data in Fig. 1. On average both phases grow approximately linearly, with the Al₂O₃ phase growing faster than the GAP phase. During several brief periods, however, the Al₂O₃ decreases in length, while the length of GAP increases. This is attributed to reactive consumption of Al₂O₃ to form GAP at the interface. It is presumed that elsewhere in the system GAP must form Al₂O₃ to supply the excess Gd³⁺ necessary to react with the Al₂O₃ at the interface as observed. The average growth rate of each phase can be measured separately, thus separate time constants may be determined using the corresponding Burger's vectors of each phase. Fig. 2b plots the instantaneous diffusivity calculated from the difference in each frame of the image sequence. The measured diffusivities vary by as much as 3 orders of magnitude as a function of time. Fig. 2c plots the angle of the interfacial plane, relative to an arbitrary reference, along with the dihedral angle averaged across the two sides of the interface as a function of time. The plotted data represent a twodimensional section of a three-dimensional object, which implies that those angles may exhibit project effects at different points in time. The average dihedral angles, nevertheless, are clearly sensitive to the inclination of the interfacial plane. An apparent correlation may exist between the dihedral angles and the calculated interfacial diffusivity, as shown in Fig. 2d, which bins and averages the diffusivity in 5° increments of dihedral angle. It is broadly anticipated that the dihedral angle increases with decreasing interfacial energy [38,39]. It may be reasonable to anticipate that, on average, interfacial diffusivity will increase with increasing interfacial energy, as is observed in grain boundaries; although this broad trend is not explicitly obeyed at every individual boundary [40-43]. The data in Fig. 2d follows the general trend anticipated: interfacial diffusivity tends to be higher for boundaries with lower dihedral angles. It should be noted that our analysis cannot account for local variations and transients in stress that may affect the measured diffusivity, and that the analysis cannot account for the interfacial torque terms that can affect the relationship between dihedral angle and interfacial energy. Experiments designed to specifically characterize interfacial anisotropy in bicrystal Coble creep will have to be the subject of future work.

Supplementary material related to this article can be found online at doi:10.1016/j.jeurceramsoc.2022.02.052.

 Al_2O_3 grain boundary creep and $Al_2O_3\text{-}GAP$ interfacial creep experiments were performed randomly at temperatures below T \approx 1628 $^{\circ}\text{C}$. The experiments we performed in sequence in the same region during progressive heating of the sample, however, above T \approx 1628 $^{\circ}\text{C}$ much of

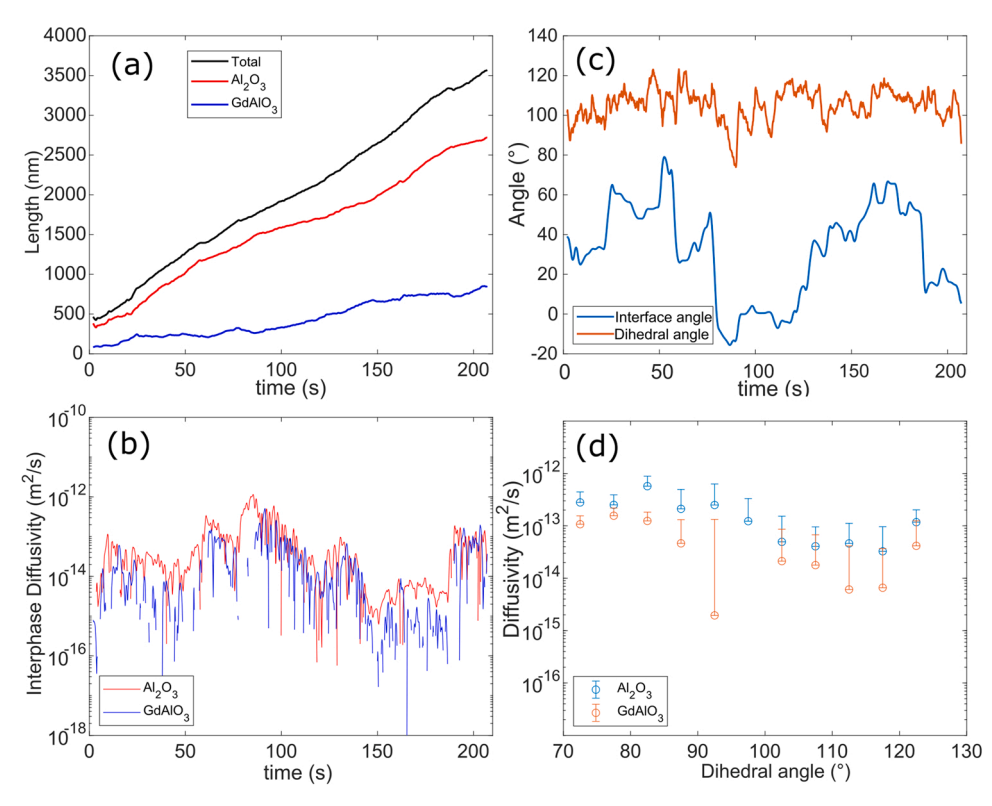


Fig. 2. Time dependent plots of (a) the length of the Al_2O_3 and $GdAlO_3$ nanowires grown by Coble creep as shown in Fig. 1, (b) the calculated instantaneous diffusivity, and (c) the angle of the interface along with the dihedral angles. (d) plots the diffusivity versus dihedral angle with experimental data binned and averaged in 5° increments of dihedral angle.

the Al_2O_3 near the surface had evaporated. Preferential Al_2O_3 evaporation was confirmed by *ex situ* SEM imaging of the sample after testing, as shown in supplementary Figure S1. GAP grain boundary creep measurements were primarily made after heating to 1674 °C and then cooling the sample down to lower temperatures. The GAP-GAP contacts were generally not favorable for creep, relative to Al_2O_3 -Al $_2O_3$ and Al_2O_3 -GAP, likely due to kinetic considerations, i.e. it is the least facile interface in the system and exhibits diffusivities close to the lower limit of what may be measured on our experimental time scales. Figs. 3 and 4 show example images of nanowires produced through Coble creep of

 Al_2O_3 grain boundaries and GAP grain boundaries at T $\approx 1628\,^{\circ}\text{C}$. The grain boundary widths of Al_2O_3 and GAP are considerably smaller than the $Al_2O_3\text{-}GAP$ interphase boundary at the same temperature, reflecting their lower relative diffusivities. The nanowire structure in Fig. 3 contains both an Al_2O_3 grain boundary and a $Al_2O_3\text{-}GAP$ interphase boundary, but the interphase boundary does not evolve significantly by creep. This difference likely results from the larger interfacial area of the interphase boundary, which causes the stress to be significantly lower than the stress on the much smaller grain boundary. The GAP-GAP necks are generally the smallest of the three interface types, and only just

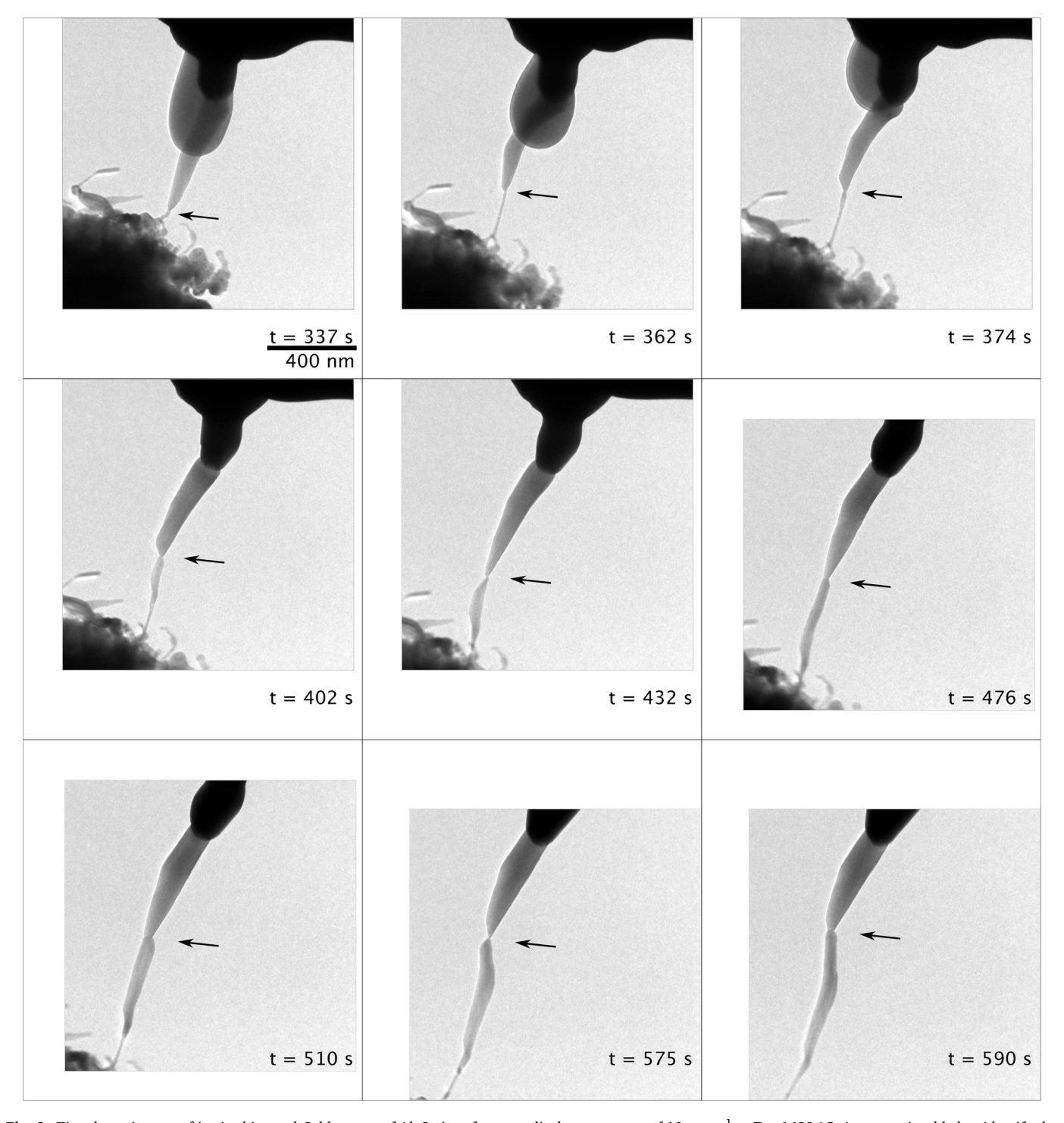


Fig. 3. Time-lapse images of in situ bicrystal Coble creep of Al_2O_3 interface at a displacement rate of 10 nm s⁻¹ at $T\approx 1628$ °C. An arrow is added to identify the interface of interest.

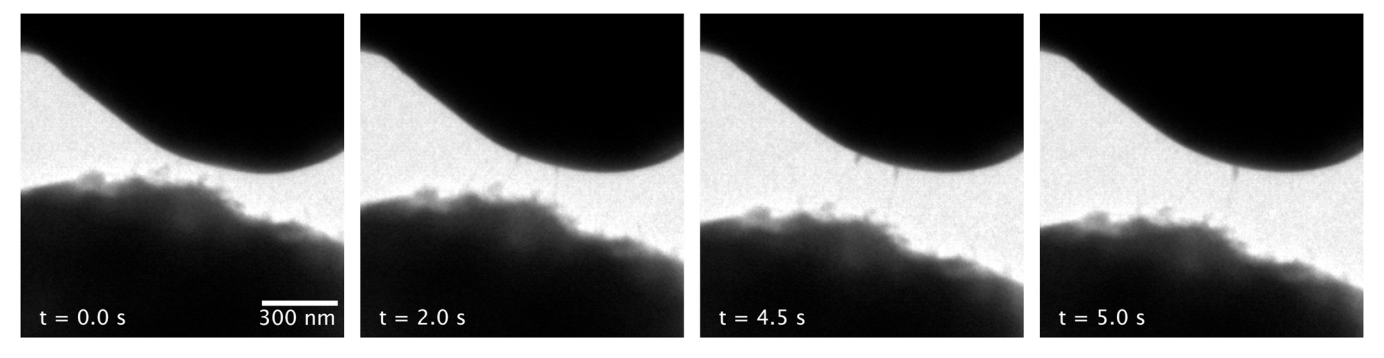


Fig. 4. Time-lapse images of in situ bicrystal Coble creep of $GdAlO_3$ interface at a displacement rate of 10 nm s⁻¹ at $T \approx 1628$ °C.

become measurable at the displacement rates used herein at $T\approx 1583\,^{\circ}\text{C}$. Eq. (2) was applied to each of the grain boundary types. Multiple separate experiments were averaged to obtain average diffusivities and standard deviations as plotted in Fig. 5. The GAP grain boundary diffusivity is the lowest, following the equation $D_{GB,GAP}=(15\pm 14)\exp\left(\frac{-580,000\pm 62,000\text{Jmol}^{-1}}{RT}\right)m^2$ s^{-1} . The alumina grain boundary diffusivity is approximately 1 order faster following the equation $D_{GB,Al_2O_3}=(25\pm 21)\exp\left(\frac{-542,000\pm 30,000\text{Jmol}^{-1}}{RT}\right)m^2$ s^{-1} . The interphase boundary, IPB, exhibits the highest diffusivity, $D_{IPB}=(15\pm 14)\exp\left(\frac{-559,000\pm 117,000\text{Jmol}^{-1}}{RT}\right)m^2$ s^{-1} . Fig. 5 shows the diffusivity in terms of the component contributions from each phase to the inter-

in terms of the component contributions from each phase to the interphase boundary. This calculation is made under the assumption that both contributions are in the diffusion limited regime, and that kinetics are not governed by the rate of nucleation of interfacial steps. This assumption is more appropriate at larger driving forces, which are anticipated to be consistent with these steady-state creep experiments. The error in the activation energy for the interphase diffusivity is large because it was calculated from the sum of the contributions from each

phase, which have different measured activation energies, $D_{IPB,GAP}$ =

$$(2.7 \times 10^{-5} \pm 2.5 \times 10^{-5}) \exp\left(\frac{-291,000 \pm 43,000 \mathrm{Jmol}^{-1}}{RT}\right) m^2$$
 s^{-1} and $D_{IPB,Al_2O_3} = (3.7 \times 10^4 \pm 3.5 \times 10^4) \exp\left(\frac{-596,000 \pm 141,000 \mathrm{Jmol}^{-1}}{RT}\right) m^2$ s^{-1} . The contributions of each phase to the diffusivity of the interphase boundary are

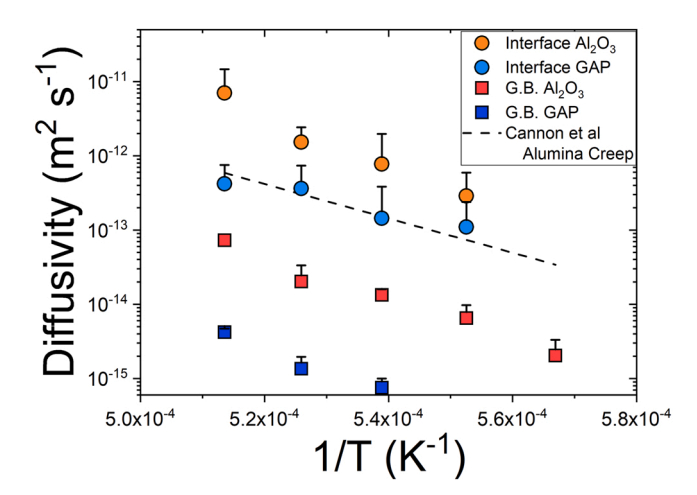


Fig. 5. Arrhenius plot of the solid-solid interfacial diffusivities in the ${\rm Al_2O_3}$ - GdAlO₃ system.

approximately 2 orders of magnitude larger than their average grain boundary diffusivities. The standard deviations associated with the interfacial diffusivity are also large, relative to the average value, as compared to the grain boundary diffusivities. As noted in the discussion of Fig. 2, significant crystallographic anisotropy is observed in the interphase boundary creep measurements, which results in a large standard deviation. Since grain boundaries can exhibit grain boundary migration it may require less thermodynamic work for the grain boundary plane to reorient away from kinetically unfavorable orientations rather than undergo long-range diffusion at a larger total applied force. If phase boundaries re-orient, however, they must do so through atomic fluxes through the boundary.

Dihedral angles were measured from the tested samples and were averaged together. The Al₂O₃-GAP interphase and Al₂O₃-Al₂O₃ grain boundary dihedral angles were measured from the growing nanowires. The GAP-GAP grain boundary dihedral angles were measured from a combination of surface groove and growing nanowire observation, since few observations of GAP-GAP nanowires were observed and their smaller size made it difficult to accurately measure dihedral angles. The surface and nanowire measurements of GAP-GAP dihedral angles were, nevertheless, reasonably consistent. The average values for the Al₂O₃- Al_2O_3 , Al_2O_3 -GAP, and GAP-GAP are $110^{\circ}\pm9^{\circ}$, $113^{\circ}\pm10^{\circ}$, and $144^{\circ} \pm 13^{\circ}$, respectively. The reported error is the standard deviation, which in part represents the width of the measured distribution, which is inherently anisotropic. The measured values are plotted in supplementary Figure S5. The relative interfacial energies derived from dihedral angle measurements are as follows, $\gamma_{Al_2O_3}>\gamma_{Al_2O_3-GAP}>\gamma_{GAP}.$ Prior dihedral angle measurements of grain boundaries and interphases in Al₂O₃-second phase systems, where the second phases were MgAl₂O₄, SiO₂, Y₃Al₅O₁₃, and CaAl₁₂O₁₉ found that the interphase boundary energy was intermediate to the grain boundaries on average in each system [44].

The surface diffusivity of each phase was measured from the rate of capillary smoothing using the analysis of Nichols and Mullins [37]. Fig. 6a and b show example capillary relaxations used to measure surface diffusivity for Al_2O_3 and GAP. Fig. 6c plots the surface diffusivities versus temperature for Al_2O_3 and GAP. The surface diffusivities of the Al_2O_3 and GAP phases can be fit to the following Arrhenius equations

$$D_{s,Al_2O_3} = \left(3.2 \mathrm{x} 10^3 \pm 2.7 \mathrm{x} 10^3\right) \mathrm{exp} \left(\frac{-539,000 \pm 26,000 \mathrm{Jmol}^{-1}}{RT}\right) m^2 \quad s^{-1} \quad \text{and} \quad S_{s,GAP} = \left(4.6 \mathrm{x} 10^4 \pm 7.7 \mathrm{x} 10^{-6}\right) \mathrm{exp} \left(\frac{-625,000 \pm 82,000 \mathrm{Jmol}^{-1}}{RT}\right) m^2 \quad s^{-1} = 0$$

respectively. It is noted that significantly fewer individual measurements were made for GAP, so the results are likely less reliable than other data reported herein. The limited number of GAP surface diffusion data points results from the fact that GAP asperities existing at the end of the creep experiment often had Al_2O_3 particles on them, which made the measurement of GAP capillary relaxations impossible. Additionally, there were fewer GAP-GAP grain boundary creep measurements than Al_2O_3 - Al_2O_3 and Al_2O_3 -GAP measurements. For this reason, no GAP

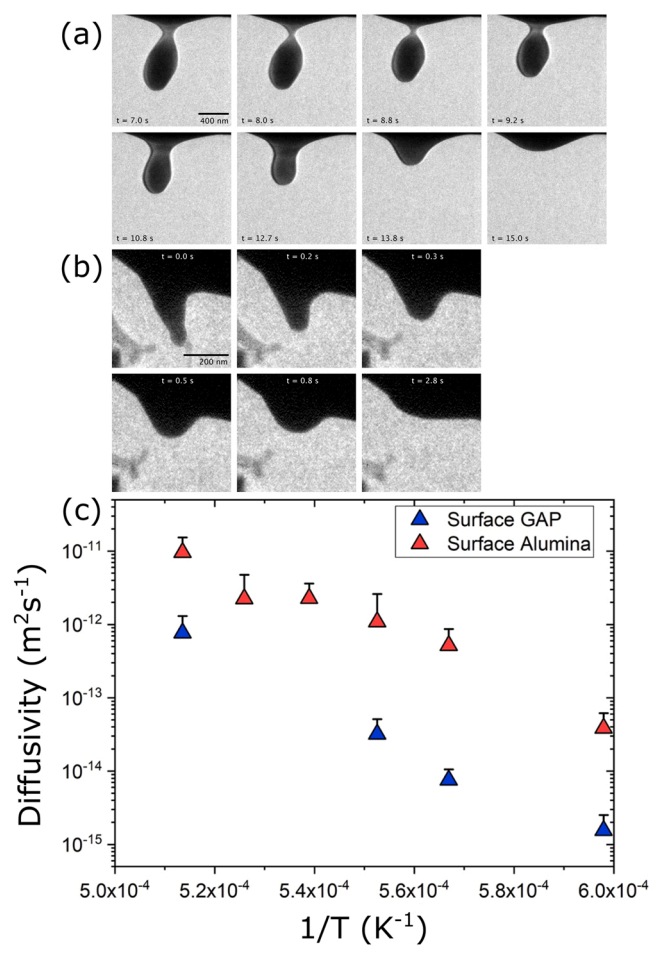


Fig. 6. Time-lapse image sequences of capillary relaxation of (a) Al_2O_3 at 1535 °C and (b) $GdAlO_3$ at 1674 °C. (c) Arrhenius plot of the surface diffusivities of Al_2O_3 and $GdAlO_3$ in vacuum.

measurements were obtained at $T=1628\,^{\circ}\text{C}$ and only one was obtained at $T=1536\,^{\circ}\text{C}$. It can be concluded, nevertheless, that Al_2O_3 surface diffusivity exceeds GAP surface diffusivity by approximately an order of magnitude. The measured surface diffusivities exceed the grain boundary diffusivities by ≈ 2 orders of magnitude. The surface diffusivities, however, are comparable to the interphase boundary diffusivity. It is noteworthy that the surface diffusivities and interface boundary diffusivities are comparable in magnitude. Since the measured interface diffusivity is not dependent on displacement length in the regime measured, it is determined that interface diffusion is rate limiting in that case despite the shorter interface path length versus apparent surface path length. Unfortunately, there is significant ambiguity regarding the rate limiting species at the different interfaces and the apparent transport paths.

4. Discussion

Cannon et al. [45] calculated diffusivities from creep of fine grained MgO-doped ${\rm Al_2O_3}$. The measured apparent activation energies fell between 410 kJ ${\rm mol}^{-1}$ and 497 kJ ${\rm mol}^{-1}$, which is slightly lower than our measurements for ${\rm Al_2O_3}$, 542 kJ ${\rm mol}^{-1}$. The calculated diffusivities are about 1 order of magnitude larger than those measured in the current work, however, MgO is anticipated to accelerate creep while rare-earth dopants are anticipated to slow creep and possibly increase the activation energy [8,15]. Rare-earth dopants have typically been associated with increasing the apparent activation energy, often to physically unrealistic values; e.g. > 800 kJ ${\rm mol}^{-1}$ [8,15]. Such high activation

energies have not generally been observed in anion and cation grain boundary diffusion measurements in rare-earth doped Al₂O₃ [46]. Those high activation energies may be indicative of mixed mechanisms as has been suggested to play an important role in the creep of polycrystalline Al₂O₃ [47]. Coble creep measurements only provide the diffusivity of the rate limiting species. The rate limiting species for Al₂O₃ grain boundary diffusion has been the subject of considerable debate since tracer measurements indicate that Al diffuses 1-2 orders of magnitude faster than O, but oxidation measurements controlled by grain boundary diffusion through Al2O3 scales typically suggest that Al diffusivity exceeds O [48-53]. It has been suggested that the mechanism for oxidation or the large chemical potential gradient during oxidation may account for this discrepancy [51,54]. Our results do not provide additional insights into this debate, but are reasonably consistent with prior creep measurements [45]. The interphase boundary Coble creep experiments indicate that the formation of new GAP phase was in some instances associated with the consumption of adjacent Al₂O₃. This combined with the fact that Al₂O₃ formation at the phase boundary is more facile than GAP formation suggest that gadolinium is likely the slow-moving species. The authors are not aware of any prior measurements of GAP grain boundary diffusivity with which to compare. The relative stability of GAP particles on Al₂O₃, as highlighted in supplementary Figure S6, suggest Gd cation diffusion on Al₂O₃ is considerably slower than both Al₂O₃ surface self-diffusion and Al cation diffusion on GAP. The result qualitatively agrees with the idea that Gd cation diffusion is slowest species at interfaces in the Al₂O₃-GAP system.

The contributions of Al_2O_3 and GAP to the interphase boundary diffusivities both exceed the grain boundary diffusivities and are comparable to the surface diffusivities. It is difficult to generalize the results, but it is interesting to note that the formation of the interphase boundary appears to be synergistic in enhancing diffusivity. As discussed in the introduction, the role of the Al_2O_3 -rare-earth aluminate boundaries in affecting creep in their composites has previously been unclear. These results suggest that the interphase boundaries do not suppress creep relative to the grain boundaries in the system. Reductions in creep rate resulting from compositing should, therefore, be attributed to some combination of topology effects that influence the diffusion pathways necessary to induce creep and doping effects at grain boundaries in the system. As noted above, rare earth dopants segregated to grain boundaries are known to dramatically suppress creep in Al_2O_3 [8,12,15].

Al₂O₃ surface diffusion measurements have been made by several researchers using a variety of techniques related to surface smoothing and thermal grooving. The reported values vary by several orders of magnitude, which could relate to the sensitivity of surface diffusivity to adsorbed impurities and environment. The magnitude of our surface diffusivities agrees reasonably well with those in References [55,56], which are later studies using higher purity materials. Prior reports of alumina surface diffusion activation energies made in similar temperature ranges as the current work fall between $\approx 460 \text{ kJ mol}^{-1}$ and $577 \ kJ \ mol^{-1} \ [56]$. The large variation, again, may relate to surface impurities, but are in line with the value measure here; 539 kJ mol⁻¹. The authors are not aware of any prior measurements of GAP surface diffusivity. The fact that GAP surface diffusion is slower than that of Al₂O₃ appears to correlate with its lower relative grain boundary diffusivity. The slower Ostwald ripening of GAP particles on Al_2O_3 relative to Al_2O_3 on GAP suggests that $Gd^{\bar{3}+}$ is the slow diffusing species in both cases.

This work demonstrates bicrystal Coble creep experiments can be used to measure interphase boundary diffusivity efficiently. Although this work focused on oxide-oxide interfaces in context of ceramic composites, the approach can be extended to a variety of materials interfaces relevant to applications such as oxidation, thin film dewetting, high temperature interfacial sliding and friction, and precipitate evolution.

5. Conclusions

This work demonstrates that bicrystal Coble creep may be used to isolate the interface diffusivities in composite materials, which are important for interpreting the response of those composite materials during processes such as creep and sintering. The results indicate that the interphase boundary diffusivity between Al₂O₃ and GdAlO₃ exceeds their individual grain boundary diffusivities by 2 orders of magnitude. The interphase boundary diffusivity is, however, comparable to the surface diffusivities. The GdAlO₃ portion of the interphase boundary creeps at a lower rate, which is consistent with GdAlO3 having a lower grain boundary and surface diffusivity than Al2O3. To the authors' knowledge, this is the first time such contributions to solid-solid interphase boundary transport have been isolated. The observation that the GdAlO₃ sometimes forms during creep through consumption of Al₂O₃ suggests that Gd³⁺ is the slow diffusing species at the interface. The results generally suggest that the lower creep rates associated with Al₂O₃-rare earth aluminate composites, relative to Al₂O₃ does not derive from a lower interphase boundary diffusivity. This effect should instead derive from composite topology and/or grain boundary doping effects.

Declaration of Competing Interest

The authors declare that they have no known competing financial interests or personal relationships that could have appeared to influence the work reported in this paper.

Acknowledgements

Support from National Science Foundation under Grant No. DMR 1922867 is acknowledged by SJD and KC. YM and J-HO acknowledge Natural Science Foundation of China for the supports in this work under Grant nos. 51572061 and 51621091 and 51972085. KH was supported by the DOE-BES Materials Science and Engineering Division under FWP 15013170. This work was performed, in part, at the Center for Integrated Nanotechnologies, an Office of Science User Facility operated for the U.S. Department of Energy (DOE) Office of Science. Sandia National Laboratories is a multi-mission laboratory managed and operated by National Technology & Engineering Solutions of Sandia, LLC, a wholly owned subsidiary of Honeywell International, Inc., for the U.S. DOE's National Nuclear Security Administration under contract DE-NA-0003525. The views expressed in the article do not necessarily represent the views of the U.S. DOE or the United States Government.

Appendix A. Supporting information

Supplementary data associated with this article can be found in the online version at doi:10.1016/j.jeurceramsoc.2022.02.052.

References

- J.E. Houser, K.R. Hebert, The role of viscous flow of oxide in the growth of selfordered porous anodic alumina films, Nat. Mater. 8 (5) (2009) 415–420.
- [2] P.Y. Hou, et al., Thermally grown Al2O3 on a H2-annealed Fe3Al alloy: stress evolution and film adhesion, Acta Mater. 55 (16) (2007) 5601–5613.
- [3] H. Barda, E. Rabkin, The role of interface diffusion in solid state dewetting of thin films: the nano-marker experiment, Acta Mater. 177 (2019) 121–130.
- films: the nano-marker experiment, Acta Mater. 177 (2019) 121–130.

 [4] J. Wang, R. Raj, Activation energy for the sintering of two-phase alumina/zirconia
- ceramics, J. Am. Ceram. Soc. 74 (8) (1991) 1959–1963.

 [5] K. Inderjeet, W. Gust, Handbook of Grain And Interphase Boundary Diffusion Data, Ziegler Press, Stuttgart, 1989, p. 1468.
- [6] A. Kumar, et al., Anomalous diffusion along metal/ceramic interfaces, Nat. Commun. 9 (1) (2018) 5251.
- [7] L. Clarisse, et al., Superplastic deformation mechanisms during creep of aluminazirconia composites, Acta Mater. 45 (9) (1997) 3843–3853.
- [8] J.D. French, et al., Creep of duplex microstructures, J. Am. Ceram. Soc. 77 (11) (1994) 2857–2865.
- [9] Y. Harada, et al., Ultra-high temperature compressive creep behavior of an in-situ Al2O3 single-crystal/YAG eutectic composite, J. Eur. Ceram. Soc. 24 (8) (2004) 2215–2222.

- [10] J. Martinez Fernandez, A. Sayir, S.C. Farmer, High temperature creep deformation of directionally solidified Al2O3/Er3Al5O12, Acta Mater. 51 (6) (2003) 1705–1720.
- [11] L. Mazerolles, et al., Creep behavior and related structural defects in Al2O3-Ln2O3 (ZrO2) directionally solidified eutectics (Ln = Gd, Er, Y), J. Eur. Ceram. Soc. 31 (7) (2011) 1219–1225.
- [12] T.A. Parthasarathy, T. Mah, L.E. Matson, Creep behavior of an alumina-YAG (Al2O3-Y3Al5O12) eutectic composite, Ceram. Eng. Sci. Proc. 11 (9–10) (1990) 1628–1638.
- [13] Y. Waku, et al., The creep and thermal stability characteristics of a unidirectionally solidified Al2O3/YAG eutectic composite, J. Mater. Sci. 33 (20) (1998)
- [14] J. Cho, et al., Improved tensile creep properties of yttrium- and lanthanum-doped alumina: a solid solution effect, J. Mater. Res. 16 (2) (2001) 425–429.
- [15] H. Yoshida, Y. Ikuhara, T. Sakuma, High-temperature creep resistance in rareearth-doped, fine-grained Al2O3, J. Mater. Res. 13 (9) (1998) 2597–2601.
- [16] M.A. Gülgün, et al., Cation segregation in an oxide ceramic with low solubility: yttrium doped α-alumina, Interface Sci. 10 (1) (2002) 99–110.
- [17] I.V. Belova, G.E. Murch, The effective diffusivity in polycrystalline material in the presence of interphase boundaries, Philos. Mag. 84 (1) (2004) 17–28.
- [18] D. Gupta, K. Vieregge, W. Gust, Interface diffusion in eutectic Pb-Sn solder, Acta Mater. 47 (1) (1998) 5–12.
- [19] F. Dyment, et al., Comparison between interphase- and grain-boundary diffusion in zirconium-based materials, Philos. Mag. A 63 (5) (1991) 959–966.
- [20] J.R. Farver, R.A. Yund, Interphase boundary diffusion of oxygen and potassium in K-feldspar/quartz aggregates, Geochim. Cosmochim. Acta 59 (18) (1995) 3607–3705
- [21] B.B. Straumal, L.M. Klinger, L.S. Shvindlerman, The effect of crystallographic parameters of interphase boundaries on their surface tension and parameters of the boundary diffusion, Acta Metall. 32 (9) (1984) 1355–1364.
- [22] J. Sommer, et al., Silver tracer diffusion in oriented AgCu interphase boundaries and correlation to the boundary structure, Acta Mater. 44 (1) (1996) 327–334.
- [23] H. Barda, E. Rabkin, Metal hetero-diffusion along the metal-ceramic interfaces: a case study of Au diffusion along the Ni-sapphire interface, Acta Mater. 186 (2020) 242–249.
- [24] R.L. Grosso, et al., Ultrahigh temperature in situ transmission electron microscopy based bicrystal coble creep in Zirconia II: Interfacial thermodynamics and transport mechanisms, Acta Mater. 200 (2020) 1008–1021.
- [25] K.S.N. Vikrant, et al., Ultrahigh temperature in situ transmission electron microscopy based bicrystal coble creep in zirconia I: Nanowire growth and interfacial diffusivity. Acta Mater. 199 (2020) 530–541.
- [26] D.-G. Xie, et al., Controlled growth of single-crystalline metal nanowires via thermomigration across a nanoscale junction, Nat. Commun. 10 (1) (2019) 4478.
- [27] C.S. Bonifacio, et al., In situ transmission electron microscopy study of dielectric breakdown of surface oxides during electric field-assisted sintering of nickel nanoparticles, Appl. Phys. Lett. 101 (9) (2012), 093107.
- [28] A. Sharma, et al., Pseudoelasticity of metal nanoparticles is caused by their ultrahigh strength, Adv. Funct. Mater. 30 (18) (2020), 1807554.
- [29] A. Henniche, et al., Effect of SiC addition on mechanical properties of hot-pressed Al2O3-GdAlO3 ceramics with eutectic composition, Ceram. Int. 44 (8) (2018) 9585–9592.
- [30] A. Henniche, et al., Microstructure and mechanical properties of ceramics obtained from chemically co-precipitated Al2O3-GdAlO3 nano-powders with eutectic composition, Ceram. Int. 43 (9) (2017) 6996–7001.
- [31] G.P. Pells, D.C. Phillips, Radiation damage of α-Al2O3 in the HVEM: I. Temperature dependence of the displacement threshold, J. Nucl. Mater. 80 (2) (1979) 207–214.
- [32] G.S. Jawaharram, et al., Irradiation induced creep in nanocrystalline high entropy alloys, Acta Mater. 182 (2020) 68–76.
- [33] R.M. Cannon, W.C. Carter, Interplay of sintering microstructures, driving forces, and mass transport mechanisms, J. Am. Ceram. Soc. 72 (1989) 1550–1555.
- [34] D. Josell, Exact solution for the zero creep load of a wire, Acta Metall. Et. Mater. 41 (7) (1993) 2179–2183.
- [35] K.L. Johnson, Contact Mechanics, Cambridge University Press, Cambridge, 1985.
- [36] J.M. McHale, et al., Surface energies and thermodynamic phase stability in nanocrystalline aluminas, Science 277 (5327) (1997) 788.
- [37] F.A. Nichols, W.W. Mullins, Morphological changes of a surface of revolution due to capillarity-induced surface diffusion, J. Appl. Phys. 36 (6) (1965) 1826–1835.
- [38] T.A. Roth, The surface and grain boundary energies of iron, cobalt and nickel, Mater. Sci. Eng. 18 (2) (1975) 183–192.
- [39] B.L. Adams, et al., Extracting grain boundary and surface energy from measurement of triple junction geometry, Interface Sci. 7 (3) (1999) 321–337.
- [40] C. Minkwitz, et al., The inclination dependence of gold tracer diffusion along a $\Sigma 3$ twin grain boundary in copper, Acta Mater. 47 (4) (1999) 1231–1239.
- [41] E. Budke, et al., Orientation dependence of 195Au and 64Cu diffusion along symmetric [001] tilt grain boundaries in Cu, Mater. Sci. Forum 207–209 (Pt. 2) (1996) 465–468.
- [42] Q. Ma, R.W. Balluffi, Diffusion along [001] tilt boundaries in the gold/silver system
 I. Experimental results, Acta Metall. Mater. 41 (1) (1993) 133–141.
- [43] T. Surholt, D.A. Molodov, C. Herzig, Orientation dependence of Ge diffusion along symmetrical [111] tilt grain boundaries in Al, Acta Mater. 46 (15) (1998) 5245-5255
- [44] S.J. Dillon, M.P. Harmer, G.S. Rohrer, Influence of interface energies on solute partitioning mechanisms in doped aluminas, Acta Mater. 58 (15) (2010) 5097–5108.

- [45] R.M. Cannon, W.H. Rhodes, A.H. Heuer, Plastic deformation of fine-grained alumina (Al2O3): I, interface-controlled diffusional creep, J. Am. Ceram. Soc. 63 (1–2) (1980) 46–53.
- [46] H. Yoshida, Y. Ikuhara, T. Sakuma, Grain boundary electronic structure related to the high-temperature creep resistance in polycrystalline Al2O3, Acta Mater. 50 (11) (2002) 2955–2966.
- [47] O.A. Ruano, J. Wadsworth, O.D. Sherby, Deformation of fine-grained alumina by grain boundary sliding accommodated by slip, Acta Mater. 51 (12) (2003) 3617–3634.
- [48] A.H. Heuer, Oxygen and aluminum diffusion in α-Al2O3: how much do we really understand? J. Eur. Ceram. Soc. 28 (7) (2008) 1495–1507.
- [49] P. Fielitz, et al., Aluminium-26 grain boundary diffusion in pure and Y-doped polycrystalline α-alumina, Acta Mater. 127 (2017) 302–311.
- [50] P. Fielitz, et al., Self-diffusion in high-purity α-Al2O3: comparison of Ti-doped, Mg-doped and undoped single crystals, J. Eur. Ceram. Soc. 41 (1) (2021) 663–668.

- [51] A.H. Heuer, et al., Alumina scale formation: a new perspective, J. Am. Ceram. Soc. 94 (s1) (2011) s146–s153.
- [52] V.K. Tolpygo, D.R. Clarke, Microstructural evidence for counter-diffusion of aluminum and oxygen during the growth of alumina scales, Mater. High Temp. 20 (3) (2003) 261–271.
- [53] W.J. Quadakkers, et al., Composition and growth mechanisms of alumina scales on FeCrAl-based alloys determined by SNMS, Appl. Surf. Sci. 52 (4) (1991) 271–287.
- [54] A.H. Heuer, M.Zahiri Azar, A disconnection mechanism of enhanced grain boundary diffusion in Al2O3, Scr. Mater. 102 (2015) 15–18.
- [55] S.J. Bennison, M.P. Harmer, Effect of magnesia solute on surface diffusion in sapphire and the role-of magnesia in the sintering of alumina, J. Am. Ceram. Soc. 73 (4) (1990) 833–837.
- [56] W. Shin, W.-S. Seo, K. Koumoto, Grain-boundary grooves and surface diffusion in polycrystalline alumina measured by atomic force microscope, J. Eur. Ceram. Soc. 18 (6) (1998) 595–600.